Validating the idea of storing electricity using a rotating body floating on the water's surface

White Paper

IT4Innovations National Supercomputing Center
VSB – Technical University of Ostrava
October 2025

VSB-TUO, IT4Innovations National Supercomputing Center, 17. listopadu 2172/15, 708 00 Ostrava-Poruba, Czech Republic

Content

1 Validating the idea of storing electricity using a rotating body floating on the water's surface

The state-of-the-art in storing electricity as kinetic energy primarily revolves around flywheel energy storage systems (FESS). These systems store electricity by converting it into kinetic energy using a spinning rotor. The rotor maintains its motion via high-speed motors, and when electricity is needed, the kinetic energy is converted back into electrical energy.

The process begins with an external power source, such as the electrical grid or a renewable source, providing energy to the system. This energy powers a motor that spins the flywheel at high speeds. As the flywheel spins, it stores energy in the form of kinetic energy. The amount of energy that can be stored depends on the mass and speed of the flywheel. The faster the flywheel spins and the heavier it is, the more energy it can store.
When energy is needed, the stored kinetic energy is converted back into electrical energy. The motor that initially spun the flywheel now acts as a generator, harnessing the rotational energy of the flywheel to produce electricity.
The benefits of FESS include a long lifespan (up to 20 years), high round-trip efficiency (often above 85%), and environmental friendliness, as the materials used are easily recyclable and do not produce harmful waste. However, they also have limitations, such as relatively high upfront costs and complexity in design and construction.

Round-trip efficiency in the context of energy storage systems refers to the ratio of the energy outputted by the system to the energy input into it, measured at the point of connection. It's expressed as a percentage and is a key performance indicator for energy storage technologies1.
Here's the formula for round-trip efficiency (RTE):

$$RTE = \frac{Energy\ Retrieved}{Energy\ Supplied} * 100\%$$

For example, if an energy storage system takes in 100 MWh of electricity and later returns 85 MWh when discharging its round-trip efficiency would be:

$$RTE = \frac{85\ MWh}{100\ MWh} * 100\% = 85\%$$

This means that 15% of the energy was lost during the storage process. A higher RTE indicates a more efficient system with less energy loss.

Different energy storage technologies have varying round-trip efficiencies. For instance, flywheels can have efficiencies between 80% to 90%, while some battery technologies range from 75% to 90%. Factors that can affect round-trip efficiency include the technology used, the storage duration, the age and condition of the system, charging and discharging rates, system design and control, temperature and most of all, the losses due to the environment.

The flywheel is often placed in a vacuum environment and mounted on magnetic bearings to reduce losses. Because the magnetic bearings and especially placing the flywheel into the vacuum

environment is very costly and limits the size of the flywheel, this study of the effect of the resistance or drag of the object moving through a fluid environment was conducted.

1.1 Drag coefficient of the rotating object

Calculating a rotating object's drag coefficient (C_d) is more complex than for a non-rotating object because the rotation influences the flow field around the object. For a non-rotating object, the drag coefficient is typically calculated using experimental data or empirical formulas. For a rotating object, additional factors like the rotational speed, surface texture, and flow regime need to be considered. However, here is a general approach to calculating the drag coefficient of a rotating object:

The drag coefficient (C_d) is generally defined as:

$$C_d = \frac{F_d}{\frac{1}{2}\rho v^2 A}$$

where:

F_d is the drag force
r is the fluid density
v is the relative velocity of the object with respect to the fluid
A is the reference area (usually the projected area of the object perpendicular to the flow direction)

For rotating objects, the drag force (F_d) and, consequently, the drag coefficient (C_d) are influenced by both translational and rotational motion. The following factors need to be considered:

Relative Velocity: The relative velocity at any point on the surface of the object will be influenced by both the translational and rotational velocities. For a rotating sphere, for example, the relative velocity can be approximated as:

$$v_{rel} = \sqrt{v^2 + (\omega r)^2}$$

where:

w is the angular velocity
r is the radius of the sphere

Magnus Effect: The Magnus effect causes a lift force perpendicular to the relative flow direction due to rotation. This can also influence the drag coefficient indirectly.

Surface Roughness and Boundary Layer Effects: Rotation can affect the boundary layer characteristics and transition points from laminar to turbulent flow, thereby influencing the drag.

1.2 Empirical or Computational Methods

Due to the complexities involved, the drag coefficient of rotating objects is often determined through:

Experimental Methods: Wind tunnel tests or other experimental setups can measure the drag force directly and compute the drag coefficient.

Computational Fluid Dynamics (CFD): CFD simulations can model the detailed flow field around a rotating object and provide insights into the drag forces and resulting drag coefficient.

2 Determination of the amount of kinetic and potential energy of a rotating hollow sphere, taking into account the free water level inside the sphere

The basic idea of storing electrical energy using a rotating body floating on the water surface is based on the well-known method of storing electrical energy in the form of kinetic energy, except that in this case, the flywheel floats on the water surface. In this particular case, it was furthermore considered that the interior of this body, more precisely a sphere, would be filled with water. In this way, both the desired mass of the body is achieved and the change in the potential energy of the free surface in the interior of the body can be used to increase the storage capacity.

Analytical relationships were used to initially determine how the change in potential energy due to the change in water level affects the total energy of a rotating sphere filled with water.

The relation for calculating the kinetic energy of a rotating body is as follows:

$$E_k = \frac{1}{2} J \omega^2$$

Where:
J is the moment of inertia of the body
w is the angular velocity

To determine potential energy due to a change in water level inside the rotating sphere we have to consider two possible states. The first state is the continuous surface solution, which is valid until the canopy of the rotating paraboloid touches the bottom of the sphere, Fig. 1.

Continuous water level - paraboloid does not touch bottom of sphere

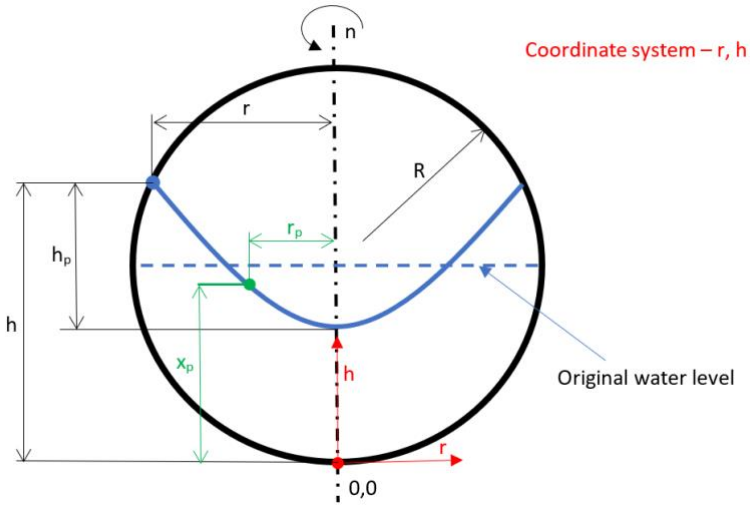

Figure 1 Continuous water level

Then the second state with a discontinuous surface is solved, which becomes valid as soon as the surface splits into two separate parts, Fig. 2.

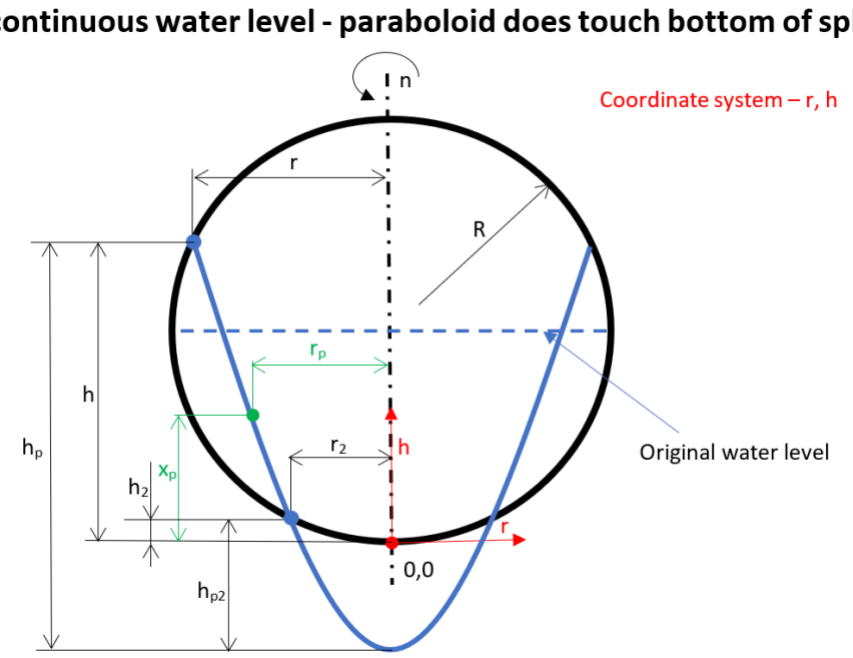

Figure 2 Noncontinuous water level

Since a continuous solution for all possible parameters such as the radius of the sphere, its angular or circumferential velocity, or the percentage of water filling of the sphere would be impractical and very lengthy, calculations were performed for a sphere with a radius of 1m, 5m, and 50m. We also limited the amount of water in the middle of the sphere by considering one-half of the sphere filled. We have also limited the range of the ball's speed so that for the ball with the largest radius (i.e. r = 50m) its circumferential speed does not exceed half the speed of sound. This condition limited the maximum number of revolutions we used for the calculations for spheres of all three radiuses to 30 revolutions per second.

Parameter	Used values
Sphere radius [m]	1, 5, 50
Water amount [%]	0 – 50
RPM	0 - 30

Table 1 Parameters for calculation of stored energies

Figure 3 shows the water level inside the sphere for a sphere with a radius of 1m and 30 rpm. From this figure, it can be seen that during the rotational motion, the level increases towards the walls of the sphere and, therefore, that there is indeed a change in potential energy.

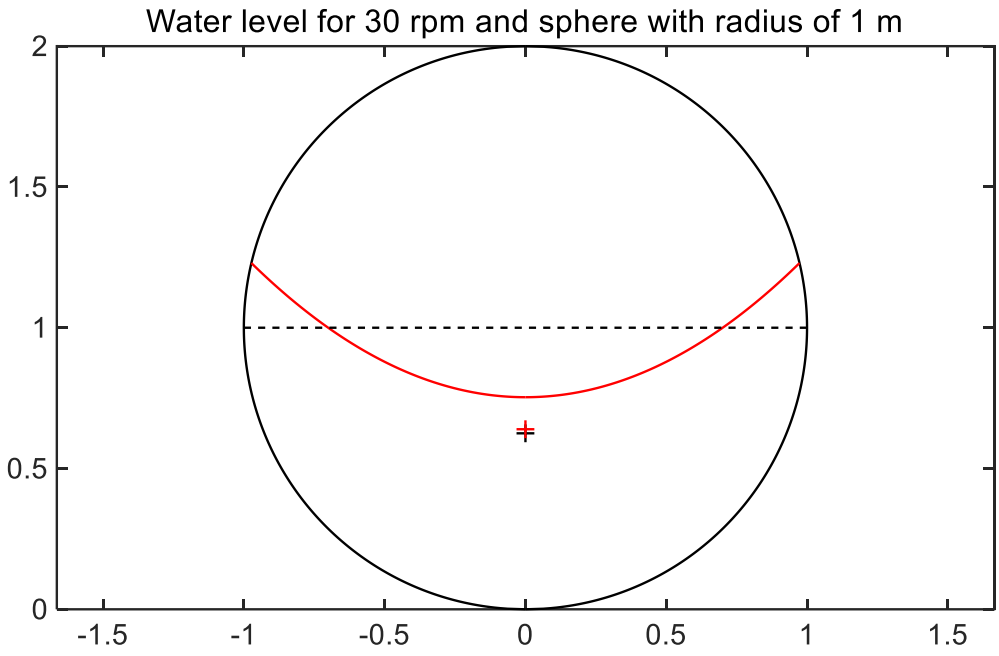

Figure 3 Water level for sphere of r=1m and 30 rpms

Since for a sphere with a radius of 1 m the limiting speed at which the circumferential velocity reaches the value of half the speed of sound is much higher, the calculation was made for a speed of 100 RPM. Figure 4 shows the water level inside the sphere for this case.

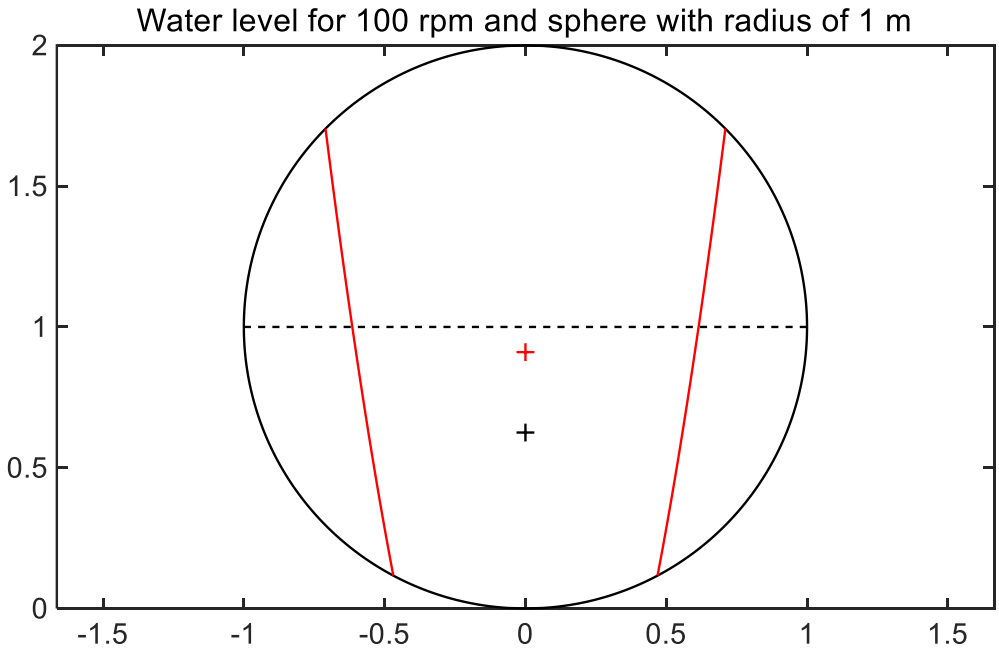

Figure 4 Water level for sphere r=1m and 100 RPMs

In both pictures, the black cross shows the centre of gravity of a ball filled with 50% water and the red cross shows the current position of the centre of gravity depending on the shape of the water level.

It can be seen that as the speed is increased, the water's centre of gravity moves to the very centre of the sphere, thus reaching the maximum potential energy. As the speed increases further,

only the kinetic energy increases. Figure 5 shows the moment of inertia, which reaches its maximum once the centre of gravity of the water surface has stabilized.

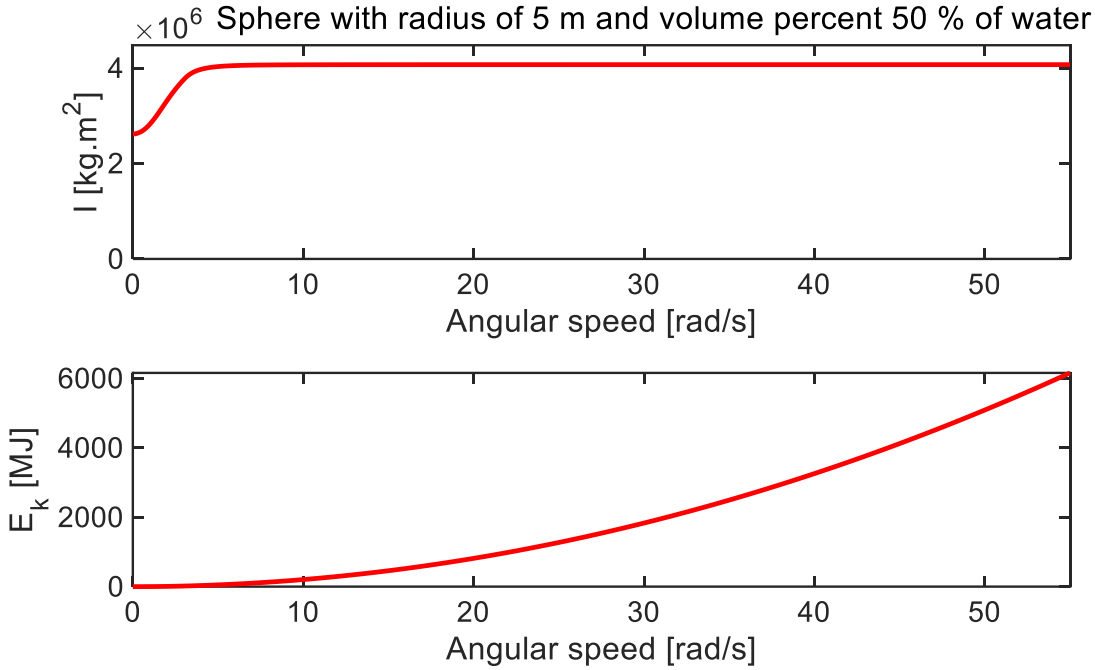

Figure 5 Moment of Inertia and Kinetic energy of the sphere r=5m

Figure 6 shows the value of potential energy versus speed and the percentage volume of water for a sphere of radius 50m. The graph shows the maximum value of potential energy that is obtained for 50% water and about 30 rpm. A higher value is no longer physically possible. The pink curve in the graph bounds the touch of the canopy of the rotating paraboloid (as explained earlier) to the bottom of the sphere.

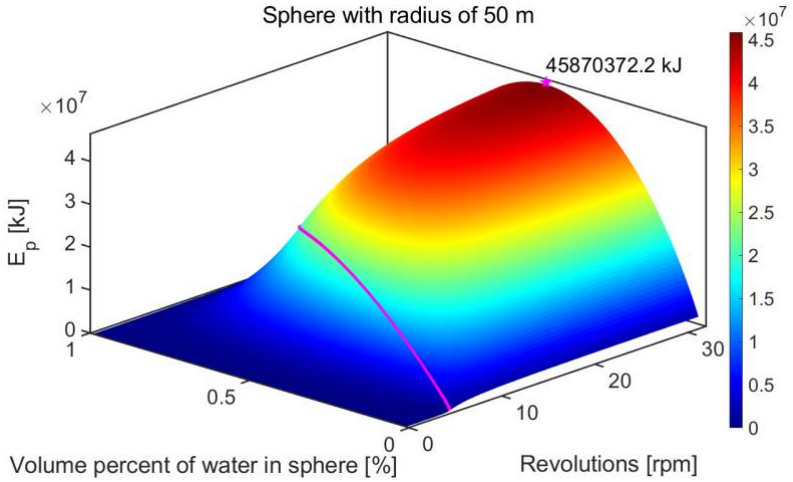

Figure 6 Potential energy of water inside of sphere r=50m

Figure 7 shows the kinetic energy as a function of the percentage of water volume and speed. It can be seen that the kinetic energy increases quadratically with increasing speed. The theoretical value of kinetic energy does not have a maximum as in the case of potential energy. The pink curve shows the touch of the canopy of the rotating paraboloid to the bottom of the sphere.

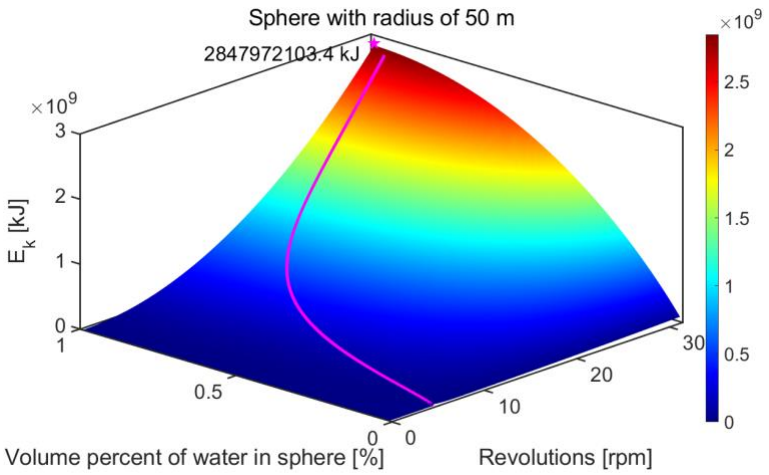

Figure 7 Kinetic energy of sphere r=50m

The resulting potential and kinetic energy values for spheres with radii of 1, 5 and 10 m are summarized in the table.

Diameter [m]	E_k [kJ]	Stored energy [kWh]	E_p [kJ]	Stored energy [kWh]
1	2 851	1	0,5	0
10	2 850 735	792	4 792	1
100	2 850 265 468	791 740	45 872 198	12 742

Table 2 Potential and Kinetic energy

It can be seen from this table that the ratio of the kinetic energy of the sphere is many orders of magnitude higher compared to the potential energy of the water surface inside the sphere, so it is not necessary to consider increasing the total energy of the rotating sphere by this potential energy.

It should be noted that the above calculations and their results were performed for an ideal condition where there are no losses such as friction losses or losses due to the movement of the sphere in a resistive environment (water, air).

3 Determination of the resistance of the rotating object using numerical modelling and simulation.

For a more realistic determination of the amount of kinetic stored in the rotating sphere, it is necessary to consider the losses due to motion in a resistive environment in the calculations. For these calculations, one of the CFD methods must already be used. In our example, the finite volume method, which is commonly used to solve such problems, was used. The ANSYS Fluent software tool was used to solve the resistive moment of sphere in a resistive environment and HPC infrastructure was leveraged to speed up the calculations.

Calculating the frictional moment (also known as the torque due to viscous forces) on a rotating object in a fluid using Computational Fluid Dynamics (CFD) involves simulating the interaction between the object and the fluid to determine the viscous forces acting on the object's surface. These forces contribute to the frictional moment, which opposes the rotation.

The frictional moment (torque) M on the rotating object due to viscous forces is computed by integrating the shear stress over the surface area A of the object:

$$M = \int_A (\mathbf{r} \times \tau)\, dA$$

Where:
r is the position vector from the axis of rotation to the point on the surface.
t is the shear stress vector.

The cross-product r × τ gives the contribution of the shear stress to the torque at each point on the surface. In a CFD simulation, this integration is performed numerically. The mesh discretizes the surface into small elements, and the shear stress on each element is multiplied by its distance from the axis of rotation and summed to compute the total frictional moment.

To compute shear stress on the object, surface the flow field around the object by solving numerically Navier-Stokes equations must be established. As mentioned earlier CFD software package ANSYS Fluent was used in our case, but any other available software could be used.

In the case of a sphere rotating on the water surface, it is necessary to take into account the type of flow from the point of view of its regime (see below) and it is also necessary to take into account the fact that part of the sphere is submerged below the water surface and part is above the water surface To be able to take this into account, we used the Volume of Fluid (VOF) method for our case.

The Volume of Fluid (VOF) method is a numerical technique used in Computational Fluid Dynamics (CFD) to track and simulate the interface between two immiscible fluids, such as air and water, within a computational domain. It is particularly useful for modelling multiphase flows where the interface between different fluids needs to be captured accurately, such as in simulations of bubbles, droplets, or waves.

The VOF method introduces a variable called the volume fraction, denoted by αwhich represents the fraction of a computational cell occupied by one of the fluids. In a two-phase system:
α =1 means the cell is entirely filled with the primary fluid (e.g., water).

α=0 means the cell is entirely filled with the secondary fluid (e.g., air).
0<α<1 indicates that the cell contains the interface between the two fluids.

The VOF method is coupled with the Navier-Stokes equations, which govern the motion of fluids. The key equation added to the standard fluid flow equations is the advection equation for the volume fraction:

$$\frac{\partial \alpha}{\partial t} + \nabla \cdot (\alpha \mathbf{u}) = 0$$

where
u is the velocity field of the fluid. This equation ensures the conservation of the volume fraction as the fluids move and interact.

The interface between the two fluids is not explicitly tracked but is instead reconstructed based on the volume fraction α values in the computational grid. Various techniques, such as the Piecewise Linear Interface Calculation (PLIC), are used to reconstruct the interface geometry within each cell, ensuring sharp and accurate representation of the interface.

Fluid properties like density ρ and viscosity μ are computed as weighted averages based on the volume fraction:

$$\rho = \alpha \rho_1 + (1 - \alpha)\rho_2$$

$$\mu = \alpha \mu_1 + (1 - \alpha)\mu_2$$

where
ρ_1, ρ_2 and μ_1, μ_2 are the densities and viscosities of the two fluids, respectively.

Surface tension effects at the fluid interface can be included in the VOF method using additional terms in the momentum equation. These terms are often modelled using the Continuum Surface Force (CSF) model, which represents surface tension as a body force acting on the fluid.

Flow regimes around objects in fluid dynamics refer to different patterns of fluid movement depending on the flow velocity, object shape, and fluid properties like viscosity. These regimes significantly influence the drag forces experienced by the objects. The primary flow regimes and their corresponding drag forces are:

1. **Laminar Flow**

In laminar flow, the fluid moves in smooth, parallel layers with minimal mixing between them. This occurs at low velocities or when the object is small, resulting in a steady and predictable flow pattern. In laminar flow, drag is primarily due to the friction between the fluid and the object's surface. The drag force in this regime is relatively low and is proportional to the velocity of the fluid and the surface area of the object.

2. **Transitional Flow**

Transitional flow is the intermediate regime between laminar and turbulent flow. It is characterized by a mix of laminar and turbulent flow patterns. Small disturbances in the flow start to grow, leading to the breakdown of the smooth layers seen in laminar flow. In the transitional regime, both viscous drag and pressure drag start to contribute to the total drag force. The drag begins to increase as turbulence starts to develop.

3. **Turbulent Flow**

In turbulent flow, the fluid exhibits chaotic and irregular motion with significant mixing and swirling. This occurs at high velocities or with larger objects where inertial forces dominate over viscous forces. In turbulent flow, the drag force is dominated by pressure drag, which results from the pressure differential between the front and rear of the object. Turbulent flow tends to create a larger wake behind the object, increasing drag. The drag force in this regime is typically higher than in laminar flow and is roughly proportional to the square of the flow velocity.

4. **Separation Flow**

Description: Flow separation occurs when the boundary layer (the layer of fluid close to the object) detaches from the surface of the object. This typically happens in turbulent flow when the object has a shape that causes the flow to slow down and reverse direction. When flow separation occurs, a large wake region with low pressure forms behind the object, leading to a significant increase in pressure drag. This is especially noticeable in bluff (non-streamlined) objects, where flow separation can drastically increase the drag force.

5. **Stagnation Flow**

Stagnation flow occurs at the point on the object where the fluid flow comes to a complete stop, usually at the leading edge or nose of the object. The pressure at the stagnation point is the highest, and this contributes to the overall pressure drag on the object. The stagnation pressure is directly related to the dynamic pressure of the flow and plays a critical role in determining the total drag force in certain cases, particularly for blunt objects.

In summary, the total drag on the object is the sum of viscous and pressure drag forces, which varies depending on the flow regime.

4 Parametric study of a object rotating on the water surface

In our case, due to the size and angular velocity of the rotating sphere, we will be in the turbulent regime and therefore the drag momentum will be directly proportional to the square of the circumferential velocity of the sphere.

At this stage, three radiuses of the rotating sphere were considered, namely 50, 100 and 200m, with the angular velocity of the rotational motion set so that the circumferential velocity of each sphere reached half the speed of sound.

Since it is very difficult to determine the exact curve of the frictional moment of a rotating ball, we considered two possible curves with the assumption that the actual curve of the frictional moment will lie somewhere between these curves. In this way, we can estimate the lower and upper limits of the resistance moment which is quite sufficient for our case.

Figure 8 shows the linear as well as quadratic characteristic of the friction torque versus angular velocity for a sphere of radius 50m.

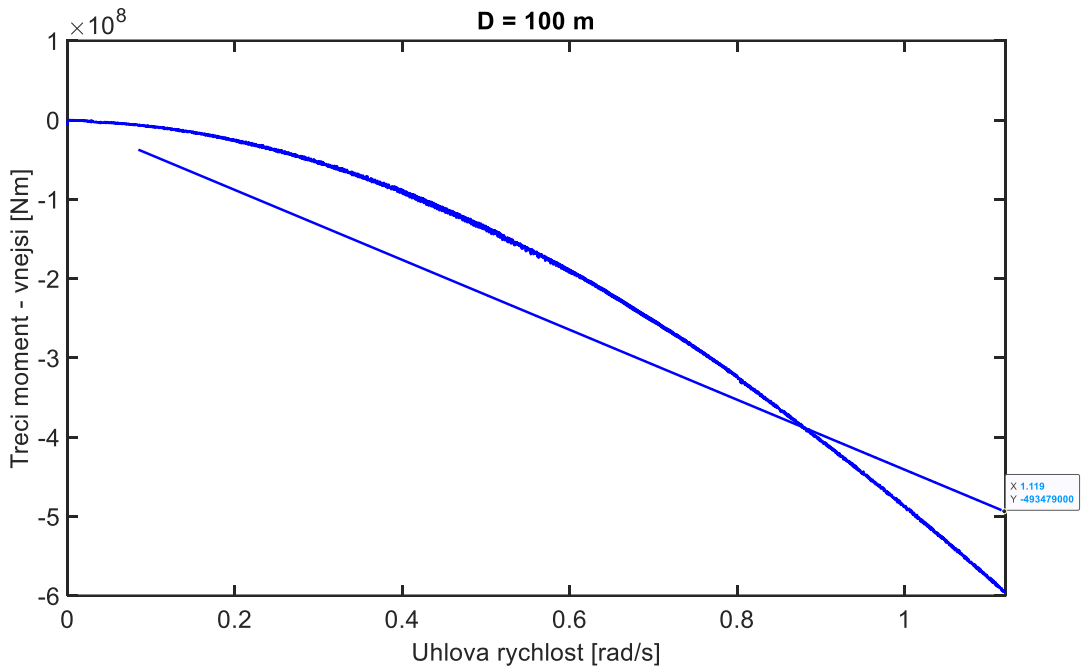

Figure 8 Linear as well as quadratic characteristic of the friction torque versus angular velocity for a sphere of radius 50m

As we already mentioned in the introductory part of this paper Round-trip efficiency is one of the important factors when it comes to energy storage. In our case, Round-trip efficiency could be referred to as a time during which the rotating sphere loses 20% of its initial kinetic energy.

In our case, it will be a time that lies between two values. The first will be determined by the case in which we consider a linear progression of the resistive moment. The second one will be the case when we consider a quadratic progression.

Figure 9 shows the angular velocity and kinetic energy as a function of time for a linear resistive moment of a sphere of radius 50m with an initial angular velocity of 3 $rad.s^{-1}$

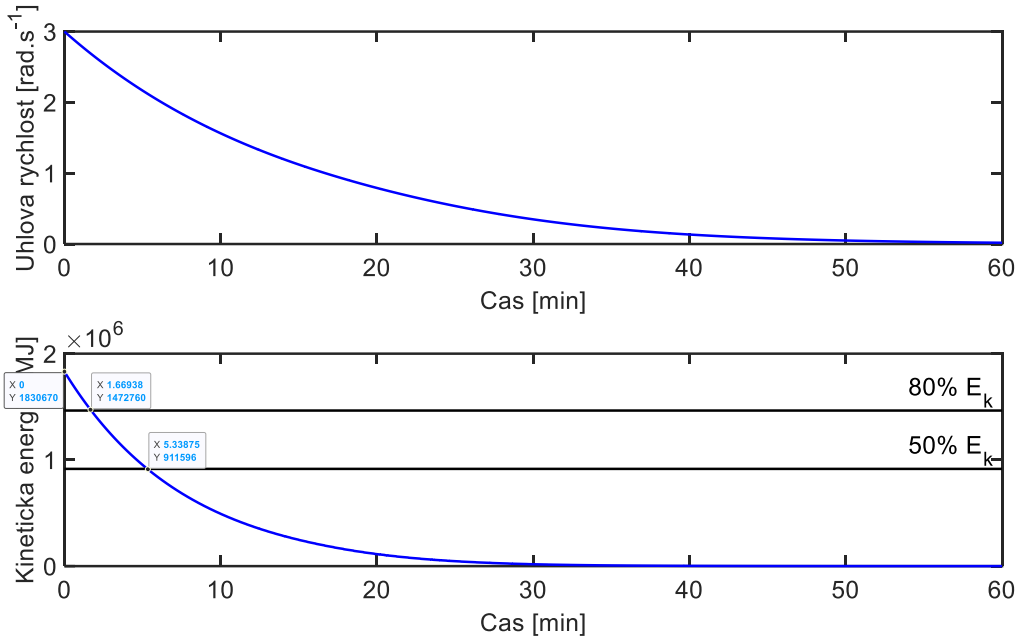

Figure 9 Angular velocity and kinetic energy as a function of time for a linear resistive moment of a sphere of radius 50m with an initial angular velocity of 3 rad.s-1

Figure 9 shows that complete stopping due to losses due to ball motion in a resistive environment occurs in about 50 minutes. The energy drops to 80% of the original value occurs in less than 2 minutes.

4.1 Parametric study of a sphere rotating in the resistant environment at a small angular velocity

The approach and methodology described above were used for a parametric study to determine how long it takes for the energy of a sphere rotating in a resistive environment to drop by 20% of its original energy. This study was carried out for three different radii of the sphere namely 50, 100, and 200 m, and for three different values of angular velocity (0.1, 0.5, and 1 rad.s^{-1})

Sphere radius [m]	Angular velocity [rad.s^{-1}]		
	0,1	0,5	1
50	7,4s	2,4s	1,7s
100	10,5s	3,5s	2,5s
200	14s	6s	4s

Table 3 The time it takes to reduce the kinetic energy of the rotating sphere by 20%

5 Effect of shape on the drag coefficient

The last study is for the different shape of the rotating body. This shape was designed to reduce the area of the body that comes into contact with the water and thus reduce frictional losses and as a result, increase the efficiency of the entire device. Figure 10 shows the new shape of the object.

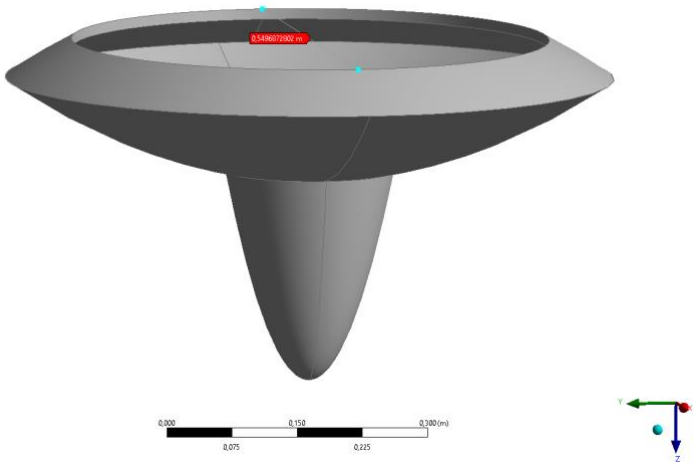

Figure 10 New shape of rotating object

For this case, an experimental measurement was carried out. The values measured in the physical experiment are shown in Tables 4 and 5.

Revolution	min	sec	hundredth	Delta	Revolution [%]	Energy [%]	Time [s]
0	0	6	12				
1	0	7	39	1,27	100	100	1,27
2	0	8	71	1,32	96,212	92,568	2,59
3	0	10	4	1,33	95,489	91,181	3,92
4	0	11	43	1,39	91,367	83,479	5,31
5	0	12	82	1,39	91,367	83,479	6,7
6	0	14	21	1,39	91,367	83,479	8,09
7	0	15	67	1,46	86,986	75,666	
8	0	17	20	1,53	83,007	68,901	
9	0	18	72	1,52	83,553	69,81	
10	0	20	24	1,52	83,553	69,81	
11	0	21	89	1,65	76,97	59,243	
12	0	23	55	1,66	76,506	58,532	
13	0	25	21	1,66	76,506	58,532	
14	0	27	0	1,79	70,95	50,339	
15	0	28	80	1,8	70,556	49,781	

Table 4 Results obtained during physical experiment

Revolution	min	sec	hundredth	Delta	Revolution [%]	Energy [%]	Time [s]
0	0	9	90				
1	0	11	36	1,46	100	100	1,46
2	0	12	82	1,46	100	100	2,92
3	0	14	34	1,52	96,053	92,261	4,44
4	0	15	87	1,53	95,425	91,059	5,97
5	0	17	47	1,6	91,25	83,266	7,57
6	0	19	6	1,59	91,824	84,316	9,16
7	0	20	71	1,65	88,485	78,296	

8	0	22	42	1,71	85,38	72,898	
9	0	24	14	1,72	84,884	72,052	

Table 5 Results obtained during physical experiment

To better display the kinetic energy progression, kinetic energy versus time plots were created and are shown in Figures 11 and 12.

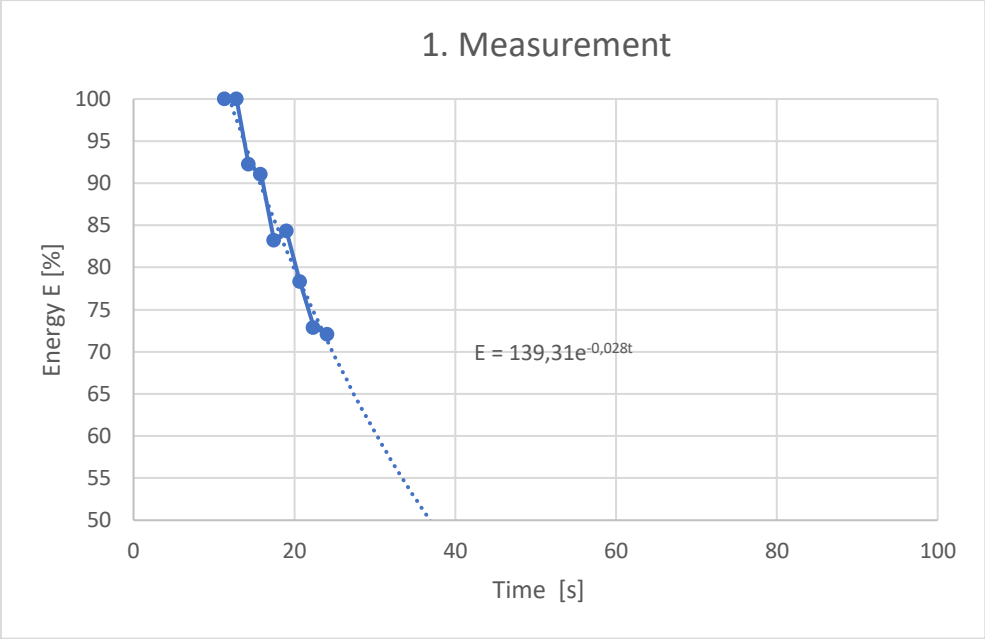

Figure 11 Kinetic energy versus time experimental measurement 1

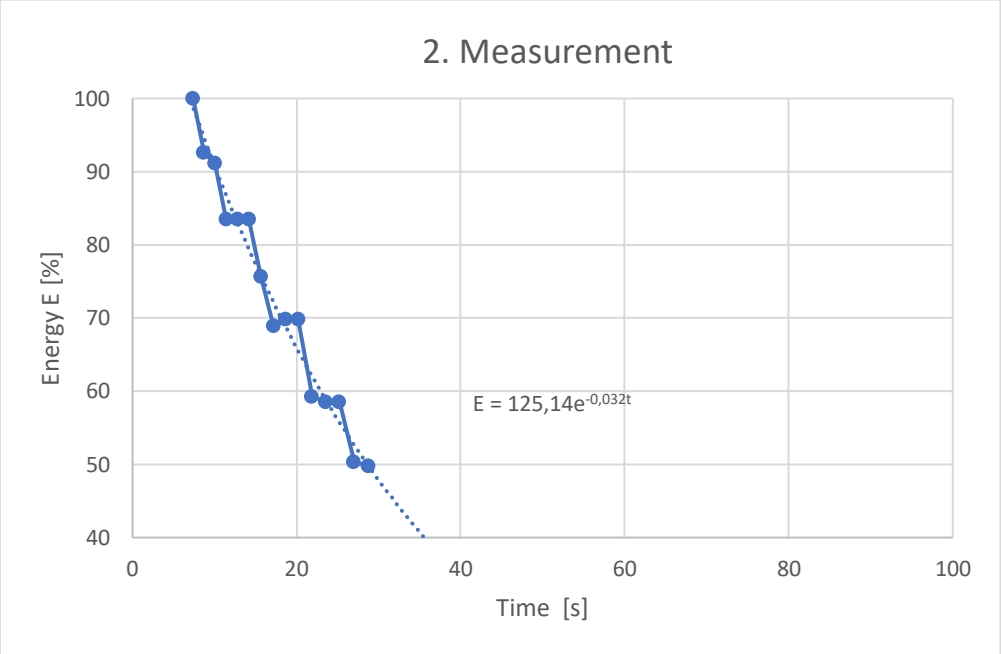

Figure 12 Figure 11 Kinetic energy versus time experimental measurement 2

For the computational part of this study, the same shape that was used in the physical experiment was used, and then calculations for a body twice or three times the size were performed.

The angular velocity was specified to be 5 rad.s^{-1} for the original body, 2.5 rad.s^{-1} for the double-sized body, and 1.25 rad.s^{-1} for the triple-sized body.

Figure 13 shows the results of the calculation of the decrease in body speed, and kinetic energy over time for the basic model. The body loses 20% of its kinetic energy in 56 seconds. For a body 2x the size (Figure 14) this is in 120 seconds and for a body 3x the size (Figure 15) it is in 230 seconds.

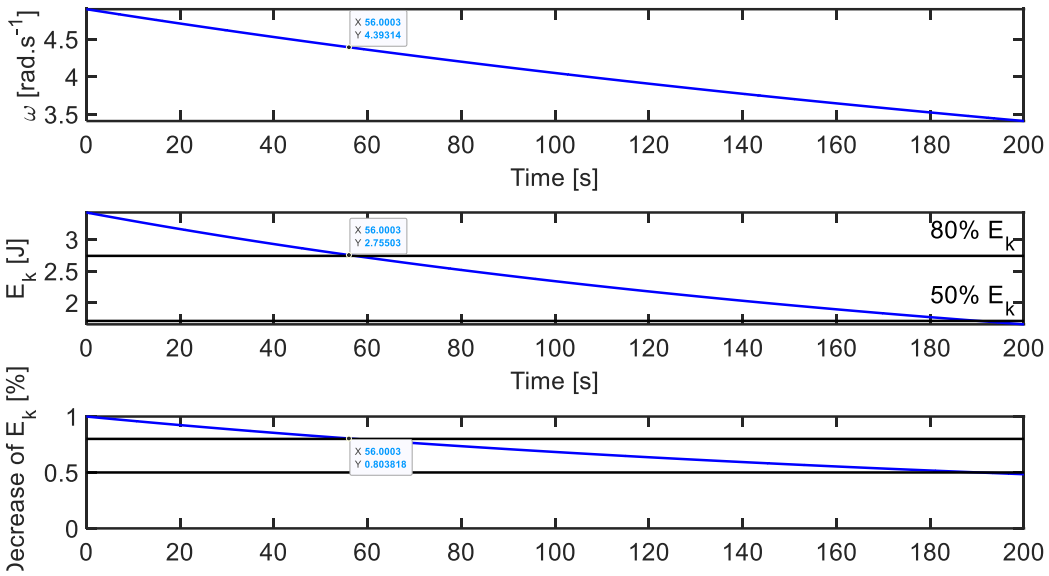

Figure 13 Decrease in body speed, and kinetic energy over time for the basic model.

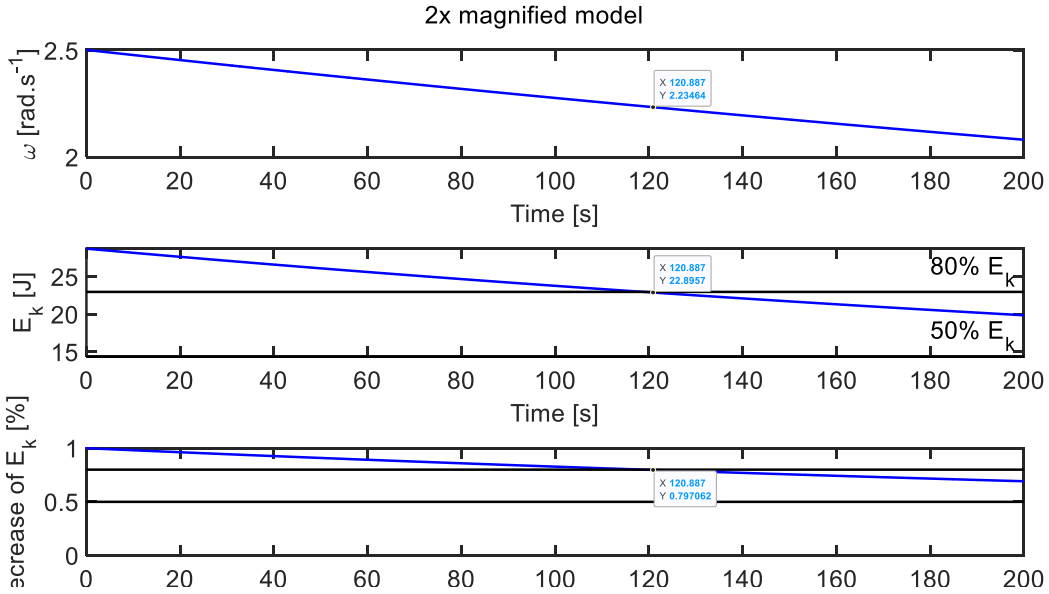

Figure 14 Decrease in body speed, and kinetic energy over time for body twice the size

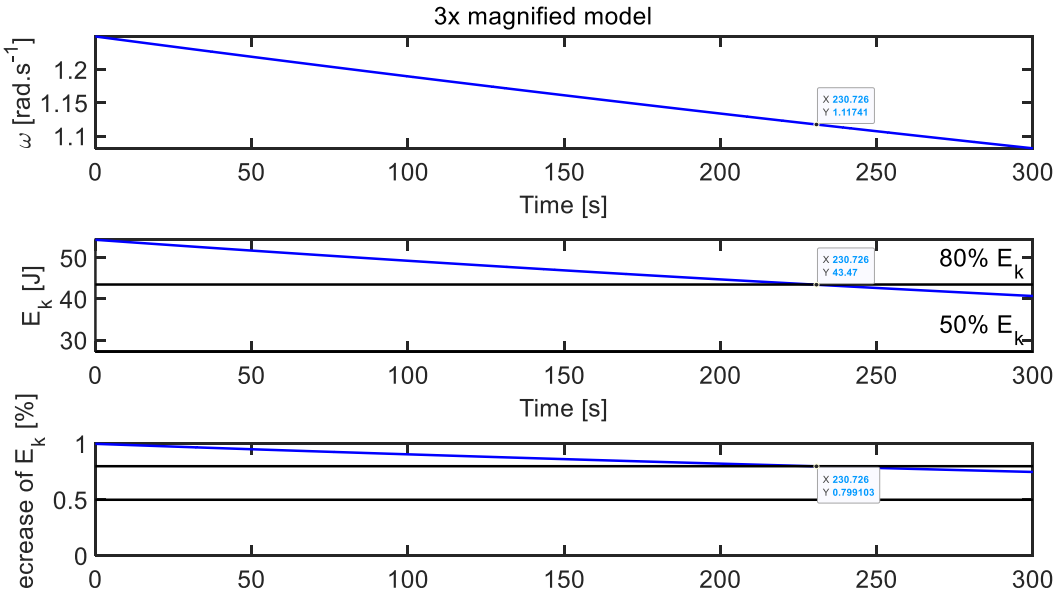

Figure 15 Decrease in body speed, and kinetic energy over time for body of triple size

By comparing the experimental results with the computational results, we see that the numerical calculation of the time during which the kinetic energy drops by 20% is significantly lower than that observed in the physical measurement. This fact is because many simplifications were made in the numerical solution and therefore some effects are not included. This fact is not detrimental since the numerical calculation is primarily used for the initial estimation of the efficiency of electrical energy storage in a body rotating on the water surface and for a possible scalability study. I.e. what would be the efficiency of a much larger body? Therefore, we do not consider these simplifications to be critical.

6 Conclusion

The aim of this document was to outline how numerical modelling and simulation methods such as CFD can be used to determine the energy loss of an object rotating on the water surface. These methods have been used primarily for the parametric study of a sphere rotating on the water surface.

This example demonstrated the possibilities and advantages of computational solutions to this problem, using which it is possible to verify the idea already in its inception without the need for its verification by experimental approach when it is necessary to build the device on which it is to verify this idea.

Another advantage of computational methods is the possibility to perform parametric studies or what-if analyses where computational methods allow us to virtually "test" many variants.

This project has received funding from the European High-Performance Computing Joint Undertaking (JU) under grant agreement No. 101101903. The JU receives support from the Digital Europe Programme and Germany, Bulgaria, Austria, Croatia, Cyprus, the Czech Republic, Denmark, Estonia, Finland, Greece, Hungary, Ireland, Italy, Lithuania, Latvia, Poland, Portugal, Romania, Slovenia, Spain, Sweden, France, the Netherlands, Belgium, Luxembourg, Slovakia, Norway, Turkey, Republic of North Macedonia, Iceland, Montenegro, and Serbia. This project has received funding from the Ministry of Education, Youth and Sports of the Czech Republic

VSB-TUO, IT4Innovations National Supercomputing Center, 17. listopadu 2172/15**,** 708 00 Ostrava-Poruba**,** Czech Republic